Materials for Renewable and Sustainable Energy (2018) 7:19
https://doi.org/10.1007/s40243-018-0126-8

ORIGINAL PAPER

Photoelectrochemical performance and carrier lifetime of electrodes based on MWCNT-templated TiO_2 nanoribbons

J. C. Calva-Yáñez[1] · M. Solís de la Fuente[2] · M. Ramírez-Vargas[2] · M. E. Rincón[2]

Received: 26 February 2018 / Accepted: 7 July 2018 / Published online: 25 July 2018

Abstract

Electron lifetime and photoelectrochemical performance of carbon-doped TiO_2 electrodes are presented. Thin films of random disposed ribbon-like structures of C-doped TiO_2 were applied onto FTO substrates using spray and dip-coating techniques. The fabricated electrodes show photocurrent enhancement 20 times greater than compact TiO_2 electrode, and electron lifetimes 2 orders of magnitude lower than compact TiO_2 films. Enhancement in photocurrent suggests a beneficial role of C-doping which compensates the transport properties expected to deteriorate in disordered and thicker architectures. Due to its large surface area, C-doped TiO_2 electrodes can be used as matrix for the deposition of QD sensitizers for photovoltaic applications or as photoanode for photocatalytic applications. Still optimization on film thickness and passivation strategies must be implemented to increase the carrier lifetime.

Keywords Electron lifetime · C-doped TiO_2 · Photon to current efficiency

Introduction

Quantum dot-sensitized solar cells (QD-SSC) based on nanocrystalline TiO_2 films are still a topic of research in recent years, [1–4] due to the feasibility of low cost photovoltaic energy conversion. These cells can be constructed by depositing small nanoparticles (quantum dots) of chalcogenide semiconductors (typically CdS, [5–7] CdSe, [8–10] and PbS [11–13]) onto a wide band gap oxide electrode such as TiO_2, in contact with an electrolyte containing appropriate redox couples, and closing the circuit with a high efficient counter electrode [14]. To increase the efficiency of sensitized solar cells (Dye and QD). The research focuses mainly on two strategies: adding an additive such as carbon nanotubes [15, 16] or graphene [17] to the electron transport layer (ETL) to improve charge collection and carriers transport, as well as its surface area to absorb a larger amount of sensitizer [18], and Shifting the photoresponse of wide band gap oxides towards the visible region to increase the efficiency of semiconductors used as photocatalyst [19]. Impurities such as C and N have been known to shift the light absorption of TiO_2 to longer wavelengths [20]. Moreover, C and N *p*-orbitals show significant overlap with the valence band O-2*p* orbitals facilitating the transport of photogenerated charge carriers onto the mesoporous TiO_2 film, improving the electron lifetime [21]. Electron lifetimes reported for solar cells based on TiO_2 films are very long in comparison to conventional solar cells, [22–24] and depend on light intensity [25]. They are controlled by the interaction of the photogenerated electrons with the oxide, obligating to a systematic study of this parameter in new materials based on impurity doped TiO_2. In this work, we present the photoelectrochemical assisted determination of electron lifetime in novel photoelectrodes based on MWCNT-templated TiO_2 nanoribbons. Our findings indicate that these electrodes are potential candidates for energy and environmental applications, although passivation and recombination studies are still needed.

✉ J. C. Calva-Yáñez
jccalva@conacyt.mx

[1] CONACyT-Centro de Graduados e Investigación en Química, Instituto Tecnológico de Tijuana, Blvd Alberto Limón Padilla S/N Col Otay, 22510 Tijuana, BC, Mexico

[2] Instituto de Energías Renovables, Universidad Nacional Autónoma de México, Privada Xochicalco S/N Temixco Mor, 62580 Mexico, Mexico

Experimental

Photoelectrodes were prepared by depositing multiwalled carbon nanotubes (MWCNT)-templated TiO_2 nanoribbons on ultrasonically cleaned FTO substrates (2 cm × 1 cm TEC7). Two dip-coating cycles based on a sol–gel solution containing titanium isopropoxide, isopropyl alcohol, water, and hydrochloric acid [$Ti(OPr^i)_4$:IPA:H_2O:HCl] were applied to FTO substrates to grow a compact film of TiO_2 (100 nm); this layer improves the adherence of subsequent films and avoids contact between the FTO and the electrolyte. Acid-treated MWCNT were deposited by spray coating on the compact TiO_2 film, using a carbon load of 0.5 mg cm^{-2}. Templated TiO_2 nanoribbons were obtained by applying nine additional dip-coating cycles and air annealing at 550 °C for 1 h. Annealing removes most of the carbon nanotubes and promotes carbon doping of the oxide film, still it preserves the template form imposed by the randomly oriented MWCNT film. Compact TiO_2 electrodes with 500 nm thickness were also fabricated by dip-coating (ten cycles) and air annealing (550 °C), for comparison.

Morphological characterization of the compact and porous electrodes was carried out by scanning electron microscopy (SEM), using a field emission microscope HITACHI S-5000. Optical characterization was performed using an UV–vis-NIR spectrophotometer Shimadzu UV-3101PC. Crystalline phases and particle size were determined with a Rigaku DMAX 2000 system. The crystal size was obtained from the Scherrer equation, using the peak at $2\theta = 25.2°$. The thickness of the TiO_2 films was measured using a Profilometer Sylus XP-200. The electrochemical and photoelectrochemical characterization was performed in a BAS CV50 electrochemical system coupled to a 100 W QTH Apex illuminator attached to a 1/8 m cornerstone 130 monochromator, with 350 nm blaze grating and 1.56 mm slits (10 nm bandpass). Cyclic voltammetry under pulsed illumination was carried out in 0.1 M Na_2SO_4, using a three-electrode cell, with Ag/AgCl as the reference electrode and graphite as the counter electrode. Impedance studies (EIS) were carried out in a potentiostat/galvanostat AUTOLAB AUT84897 system.

Results and discussion

Figure 1a shows FE-SEM images of the ribbon-like structure of C-doped TiO_2 electrodes. At higher magnification (Fig. 1b), it is possible to observe a semi-rolled ribbon structure produced by the combustion of the carbon nanotubes due to the high annealing temperature in air (550 °C). Crystal size of the agglomerated elliptical particles is in the range of 13–16 nm, and the thickness of the TiO_2 shell is estimated in 20 nm. Thickness of TiO_2 and C-doped TiO_2 films obtained by profilometry was 0.5 and 15 microns, respectively.

XRD patterns for porous C-doped TiO_2 and compact TiO_2 electrodes are shown in Fig. 2a. Diffraction peaks for compact TiO_2 films correspond only to anatase, since no other phases are evident. Anatase (101) is also the dominant plane in C-doped TiO_2, although SnO_2 (110) plane is also present at $2\theta = 26.4°$ and corresponds to the TCO substrate; graphitized planes are not evident, confirming the complete combustion of CNTs. Average crystallite size of anatase was estimated in 15 and 17 nm in compact and porous C-doped films, respectively. Figure 2b shows the determination of indirect band gap (E_g) estimated from the absorption coefficient spectra (α) obtained from Eq. (1), in terms of transmittance and reflectance spectra (not shown) assuming multiple reflections; E_g was estimated on 3.18 eV for compact TiO_2 electrode and 2.83 eV for C-doped TiO_2 electrodes. The photoresponse of these electrodes was measured at positive bias (0 V vs E_{ref}) and 25 mW cm^{-2} of illumination intensity, making evident a 20× increase in porous C-doped films relative to compact films (Fig. 3). Apparently, the improvement in photocurrent is due to the enhancement in surface area that occurs without detriment of the oxide crystallinity. It can also be intuited by the way in which the photocurrent curve falls that there is a faster electron–hole recombination in C-doped TiO_2 relative to TiO_2 electrode; this will be corroborated later with the determination of electron lifetimes.

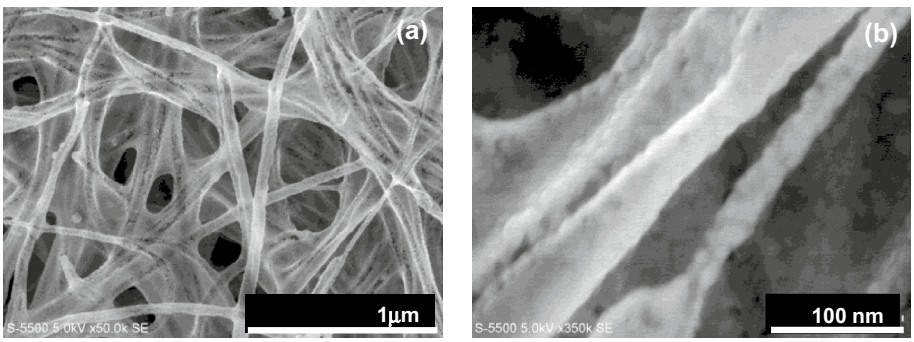

Fig. 1 **a** FE-SEM image of porous C-doped TiO_2 film annealed at 550 °C. **b** FE-SEM image of the agglomerated particles forming the open shell TiO_2 structure

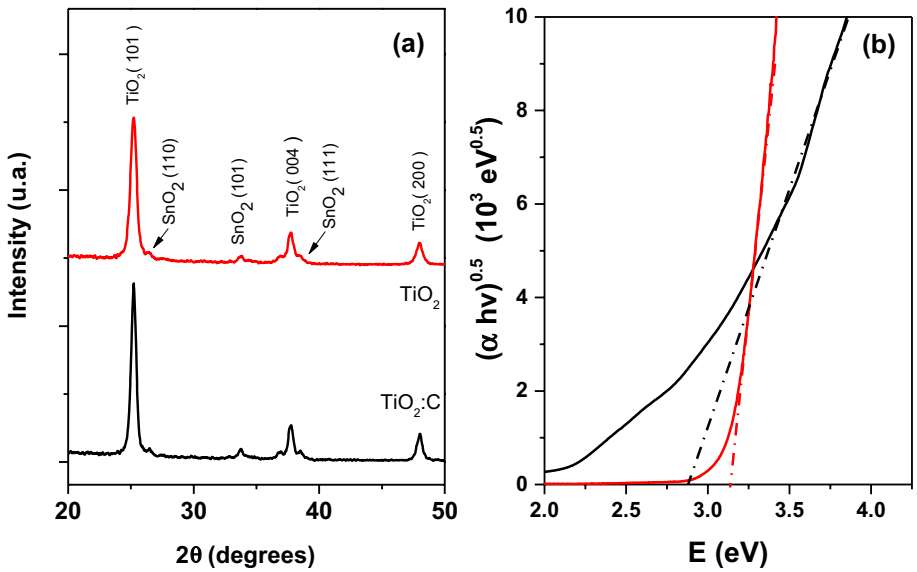

Fig. 2 **a** XRD patterns of analyzed electrodes. **b** Indirect band gap determination from absorption coefficient spectra, C-doped TiO_2 (black), compact TiO_2 (red)

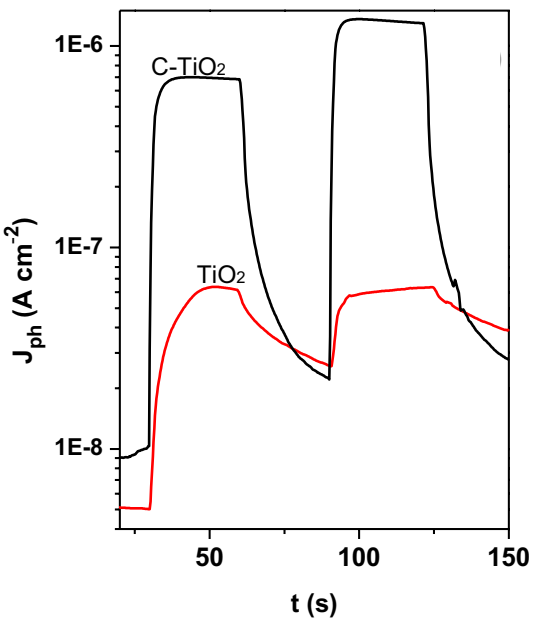

Fig. 3 Photoresponse measured at 0 V under 25 mA cm^{-2} illumination intensity, C-doped TiO_2 (black), compact TiO_2 (red)

$$\propto d = \ln\left[\frac{(1-R)^2 + \sqrt{(1-R)^4 + 2RT^2}}{2T}\right] \quad (1)$$

Figure 4 shows the spectral response and the incident photon to current efficiency (IPCE) of C-doped TiO_2 and compact TiO_2 electrodes under illumination. Higher photocurrent intensity and a red shifted spectral response are observed in C-doped material (Fig. 4a), confirming the sensitization expected from C-doping. At 350 nm, IPCE is 8 and 2.7% for C-doped TiO_2 and compact TiO_2 electrodes, respectively.

To investigate the electron lifetime of C-doped TiO_2 electrodes, electrochemical impedance spectra (EIS) were obtained in the frequency range of 40 kHz to 0.1 Hz and perturbation amplitude of 10 mV. To induce a change in the Fermi level of the analyzed electrodes, a DC-bias was applied in the range of 0–0.4 V vs OCV (open circuit voltage). Electron lifetime (τ_n) can be determined from Eq. (2), using the measured recombination resistance R_{rec} and chemical capacitance Cμ described by Eqs. (3) and (4) [25].

$$\tau_n = R_{rec} C_\mu^{cb} \quad (2)$$

$$R_{rec} = \frac{k_B T}{q^2 AL} \tau_n n_c^{-1}(V_{app}) \quad (3)$$

$$C_\mu^{cb} = \frac{q^2 AL}{k_B T} n_c(V_{app}) \quad (4)$$

where k_B is the Boltzmann's constant, T is the temperature, q is the electron charge, L is the film thickness, A is the electrode area, τ_n is the electron lifetime and n_c is the conduction band electron density as a function of applied bias.

Figure 5 shows the Nyquist plots for C-doped TiO_2 electrodes, recorded from 0 to 0.4 V applied potential. Impedance spectra were fitted using the equivalent circuit model reported by Bisquert et al. [25]. C-doped TiO_2 electrodes (Fig. 5b) show two RC semicircles (i.e., a resistor and constant phase element in parallel); the high frequency arc is related to the process taking place at the counter electrode

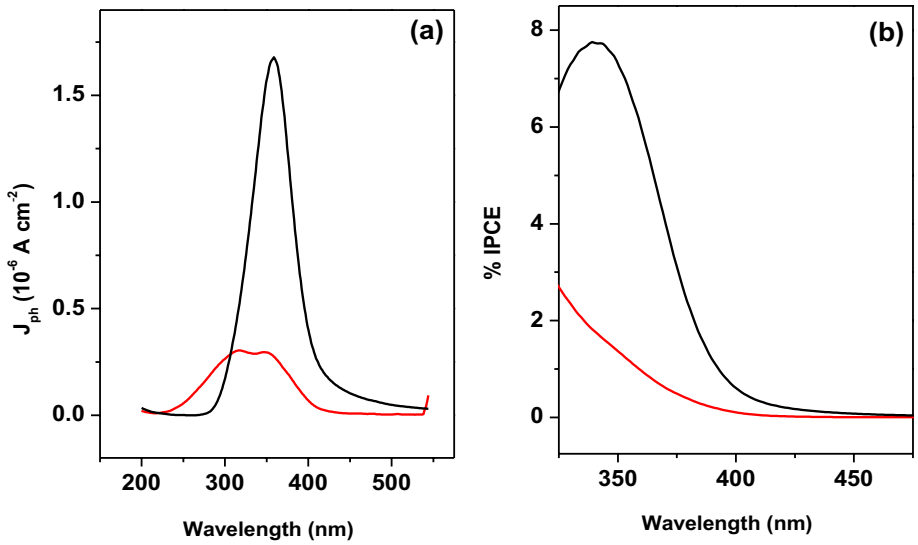

Fig. 4 **a** Spectral response of the analyzed electrodes carried out in 0.1 M of Na_2SO_4. **b** IPCE of C-doped TiO_2 (black) and compact TiO_2 electrodes (red)

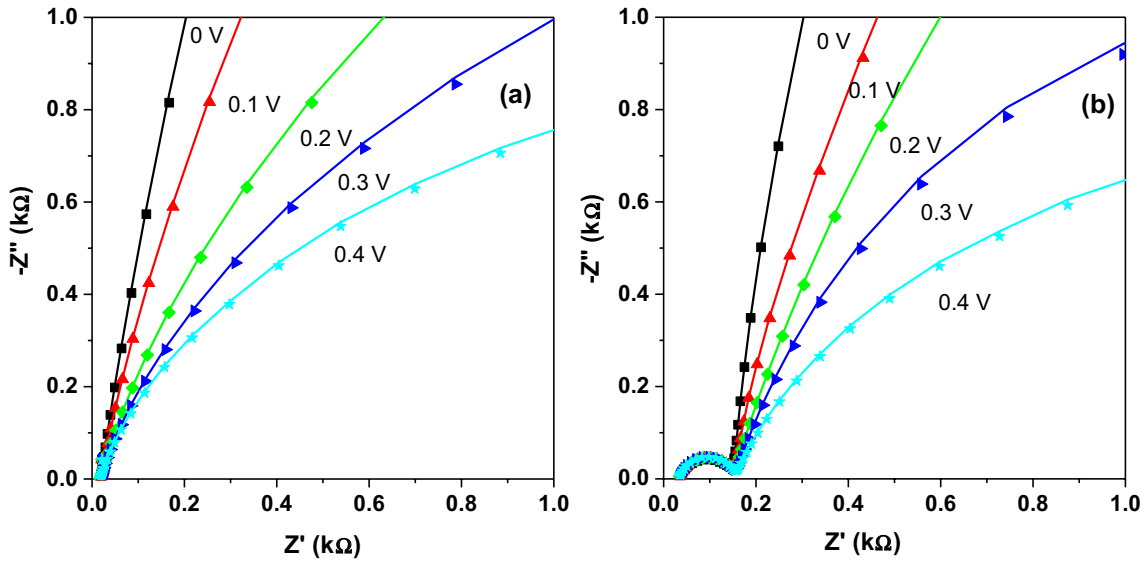

Fig. 5 Nyquist plots of impedance spectroscopy recorded from 0 to 0.4 V. **a** compact TiO_2 and **b** C-doped TiO_2

and the middle frequency arc to transport and electronic recombination in the porous TiO_2 electrode. Compact TiO_2 films show a single RC arc (Fig. 5a); interestingly, its low surface area causes little polarization in the counter electrode making the high frequency arc disappear.

Recombination resistance and chemical capacitance of C-doped and compact TiO_2 electrodes are presented in Fig. 6. Difference between recombination resistances is not significant in both electrodes (Fig. 6a), indicating similar recombination rates regardless of the different geometry and doping effect imposed by carbon. Figure 6b shows chemical capacitances that are almost insensitive to the bias applied in C-doped TiO_2, warning about the validity of the model in this material. Nevertheless, as a first approximation, we can consider a lower chemical capacitance for C-doped electrode relative to the compact film.

Life times as a function of the potential applied are shown in the Fig. 7. They are in the order of ms in C-TiO_2 electrodes and *s* for compact film TiO_2, to improve the low τ_n in nanoribbon TiO_2, a blocking layer or passivating film is suggested to decrease the recombination rate and enhanced the photovoltaic performance. Similarly, optimization of the carbon film used for C-TiO_2 electrodes has been reported to be critical for photocatalytic applications and could also be relevant for improving electron lifetime.

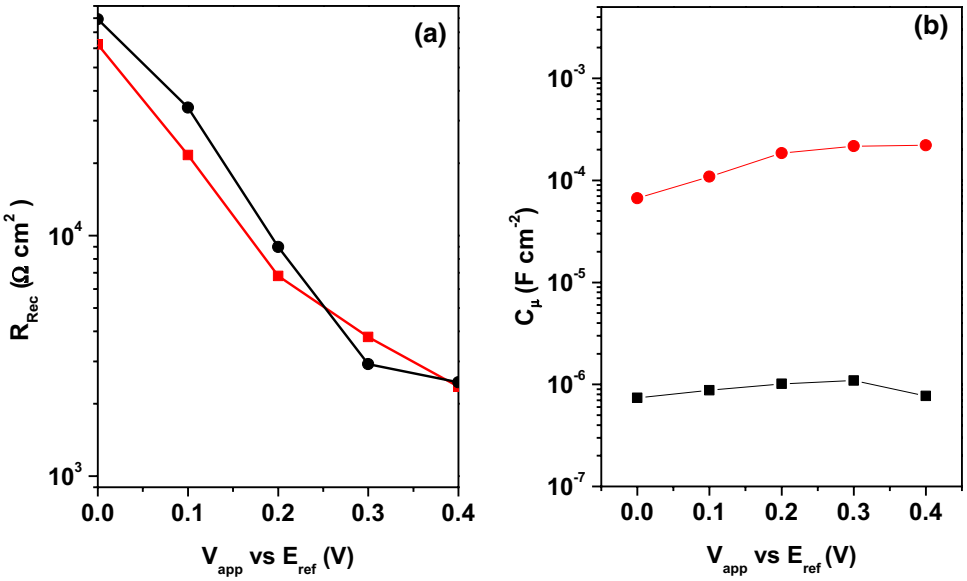

Fig. 6 Plots of the measured **a** recombination resistance and **b** chemical capacitance of the analyzed electrodes at different bias, C-doped TiO_2 (black), compact TiO_2 (red)

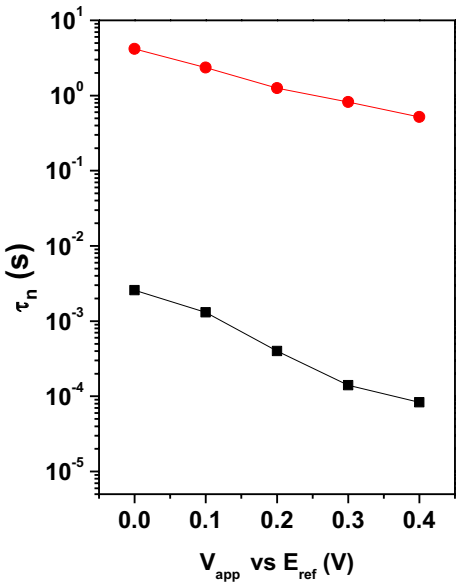

Fig. 7 Electron lifetime of the analyzed electrodes determined at different bias

Conclusions

Synthesis of porous C-doped TiO_2 electrodes by low cost methods is reported. High values of photocurrent in C-doped TiO_2 electrode are correlated with the increase in surface area that does not compromise TiO_2 crystallinity. C-doped TiO_2 electrodes and compact TiO_2 films show electron lifetimes in order of ms and s, respectively. The low value of electron lifetime in C-doped TiO_2 is due to the low value of chemical capacitance obtained as a first approximation. Nevertheless, passivation and recombination studies are in progress to increase the potential of C-doped TiO_2 matrix as a viable option for photo-anodes in solar energy conversion due to its large photocurrent and recombination resistance.

Acknowledgement To R. Morán and P. Altuzar for technical assistance, and to Projects DGAPA (IN103718) and CONACyT (245754 and 270810)—México for financial support.

References

1. Jun, H.K., Careem, M.A., Arof, A.K.: Quantum dot-sensitized solar cells-perspective and recent developments: a review of Cd chalcogenide quantum dot as sensitizers. Renew. Sust. Energy Rev. **22**, 148–167 (2013)
2. Sharma, D., Jha, R., Kumar, S.: Quantum dot sensitized solar cells: recent advances and future perspectives in photoanode. Sol. Energy Mater. Sol. Cells **155**, 294–322 (2016)
3. Yu, J., Wang, W., Pan, Z., Du, J., Ren, Z., Xue, W., Zhong, X.: Quantum dot sensitized solar cells with efficiency over 12% based on tetraethyl orthosilicate additive in polysulfide electrolyte. J. Mater. Chem. A. **5**, 14124–14133 (2017)
4. Ye, M., Gao, X., Hong, X., Liu, Q., He, C., Lui, X., Lin, C.: Recent advances in quantum dot-sensitized solar cells: insights into photoelectrodes, sensitizers, electrolytes and counter electrodes. Sustain. Energy Fuels **1**, 1217–1231 (2017)
5. Lee, H., Leventis, H.C., Moon, S.-J., Chen, P., Ito, S., Haque, S.A., Torres, T., Nuesch, F., Geiger, T., Zakeerunddin, S.M., Gratzel, M., Nazeeruddin, MdK: PbS and CdS quantum dot-sensitized solid state solar cells: "old concepts, new results". Adv. Funct. Mater **19**, 2735–2742 (2009)

6. Li, L., Yang, X., Gao, J., Tian, H., Zhao, J., Hagfeld, A., Sun, L.: Highly efficient CdS quantum dot-sensitized solar cells based on a modified polysulfide electrolyte. J Am Chem Soc **133**, 8458–8460 (2011)
7. Wang, C., Jiang, Z., Wei, L., Chen, Y., Jiao, J., Eastman, M., Liu, H.: Photosensitization of TiO_2 nanorods with CdS quantum dots for photovoltaic applications: a wet chemical approach. Nano Energy **1**, 440–447 (2012)
8. Kamat, P.V.: Quantum dot solar cells. Semiconductor nanocrystals as light harvesters. J. Phys. Chem. C **112**, 18737–18753 (2008)
9. Bang, J.H., Kamat, P.V.: Quantum dot sensitized solar cells. A tale of two semiconductor nanocrystals: CdSe and CdTe. ACS Nano **3**(6), 1467–1476 (2009)
10. Lai, Y., Lin, Z., Zheng, D., Chi, L., Du, R., Lin, C.: CdSe/CdS quantum dots co-sensitized TiO_2 nanotube array photoelectrode for highly efficient solar cells. Electrochem. Acta **79**, 175–181 (2012)
11. Ju, T., Graham, R.L., Zhai, G., Rodriguez, Y.W., Brezze, A.J., Yang, L., Alers, G.B., Carter, S.A.: High efficiency mesoporous titanium oxide PbS quantum dot solar cells at low temperature. Appl. Phys. Lett. **97**, 043106 (2010)
12. Mali, S.S., Desai, S.K., Kalagi, S.S., Betty, C.A., Bhosale, P.N., Devan, R.S., Ma, Y.-R., Patil, P.S.: PbS quantum dot sensitized anatase TiO_2 nanocorals for quantum dot-sensitized solar cell applications. Dalton Trans. **41**, 6130 (2012)
13. Zhou, N., Chen, G., Zhang, X., Cheng, L., Lou, Y., Li, D., Meng, Q.: Highly efficient PbS/CdS co-sensitized solar cells based on photoanodes with hierarchical pore distribution. Electrochem. Comm. **20**, 97–100 (2012)
14. Tachan, Z., Shalom, M., Hod, I., Ruhle, S., Tirosh, S., Zaban, A.: PbS as highly catalytic counter electrode for polysulfide-based quantum dot solar cells. J. Phys. Chem. C **115**, 6162–6166 (2011)
15. Brown, P., Takechi, K., Kamat, P.V.: Single-walled carbon nanotube scaffolds for dye sensitized solar cells. J. Phys. Chem. C **112**, 4776–4782 (2008)
16. Chen, J., Li, B., Zheng, J., Zhao, J., Zhu, Z.: Role of carbon nanotubes in dye-sensitized TiO_2-based solar cells. J. Phys. Chem. C **116**, 14848–14856 (2012)
17. Kim, S.B., Park, J.Y., Kim, ChS, Okuyama, K., Lee, S.E., Jang, H.D., Kim, T.: Effects of graphene in dye-sensitized solar cells based on nitrogen doped TiO_2 composite. J. Phys. Chem. C **119**, 16552–16559 (2015)
18. Archana, J., Harish, S., Sabarinathan, M., Navaneethan, M., Ponnusamy, S., Muthamizhchelvan, C., Shimomura, M., Ikeda, H., Aswal, D.K., Hayakawa, Y.: Highly efficient dye-sensitized solar cell performance from template derived high surface area mesoporous TiO_2 nanospheres. RCS Adv. **6**, 68092–68099 (2016)
19. Chen, X., Burda, C.: The electronic origin of the visible-light absorption properties of C-, N- and S-doped TiO_2 nanomaterials. J. Am. Chem. Soc. **130**, 5018–5019 (2008)
20. Wu, G., Nishikawa, T., Ohtani, B., Chen, A.: Synthesis and characterization of carbon doped TiO_2 nanostructures with enhanced visible light response. Chem. Mater. **19**, 4530–4537 (2006)
21. Enache, C.S., Schoonman, J., Van der Krol, R.: The photoresponse of iron- and carbon-doped TiO_2 (anatase) photoelectrodes. J. Electroceram. **13**, 177–182 (2004)
22. Fabregat-Santiago, F., Garcia-Belmonte, G., Bisquert, J., Zaban, A., Salvador, P.: Decoupling of transport, charge storage and interfacial charge transfer in the nanocrystalline TiO_2/electrolyte system by impedance methods. J. Phys. Chem. C **106**, 334–339 (2002)
23. Oekermann, T., Zhang, D., Yoshida, T., Minoura, H.: Electron transport and back reaction in nanocrystalline TiO_2 films prepared by hydrothermal crystallization. J. Phys. Chem. B. **108**, 2227–2235 (2004)
24. Green, A.N.M., Palomares, E., Haque, S.A., Kroon, J.M., Durrant, J.R.: Charge transport versus recombination in dye-sensitized solar cells employing nanocrystalline TiO_2 and SnO_2 films. J. Phys. Chem. B **109**, 12525–12533 (2005)
25. Bisquert, J., Fabregat-Santiago, F., Mora-Seró, I., Garcia-Belmonte, G., Giménez, S.: Electron lifetime in dye-sensitized solar cells: theory and interpretation of measurements. J. Phys. Chem. C **113**, 17278–17290 (2009)